HHS Public Access

Author manuscript

Gastroenterology. Author manuscript; available in PMC 2023 March 01.

Published in final edited form as:

Gastroenterology. 2022 March ; 162(3): 890–906. doi:10.1053/j.gastro.2021.11.037.

The origin and contribution of cancer-associated fibroblasts in colorectal carcinogenesis

Hiroki Kobayashi[1,2,3,4,*], **Krystyna A. Gieniec**[1,2,*], **Tamsin RM. Lannagan**[1,2,*], **Tongtong Wang**[1,2], **Naoya Asai**[5], **Yasuyuki Mizutani**[3,6], **Tadashi Iida**[3,6], **Ryota Ando**[3], **Elaine M. Thomas**[1,2], **Akihiro Sakai**[3], **Nobumi Suzuki**[1,2,7], **Mari Ichinose**[1,2], **Josephine A Wright**[2], **Laura Vrbanac**[1,2], **Jia Q Ng**[1,2], **Jarrad Goyne**[1,2], **Georgette Radford**[1,2], **Matthew J. Lawrence**[8], **Tarik Sammour**[1,2,8], **Yoku Hayakawa**[7], **Sonja Klebe**[9], **Alice E. Shin**[10], **Samuel Asfaha**[11], **Mark L. Bettington**[12,13,14], **Florian Rieder**[15,16], **Nicholas Arpaia**[17,18], **Tal Danino**[18,19], **Lisa M. Butler**[1,2], **Alastair D. Burt**[1,20], **Simon J. Leedham**[21], **Anil K. Rustgi**[18], **Siddhartha Mukherjee**[22], **Masahide Takahashi**[3,4,23], **Timothy C. Wang**[22], **Atsushi Enomoto**[3,25], **Susan L. Woods**[1,2,25,26], **Daniel L. Worthley**[2,24,25]

[1]Adelaide Medical School, University of Adelaide, Adelaide, SA, 5000, Australia

[2]South Australian Health and Medical Research Institute (SAHMRI), Adelaide, SA, 5000, Australia

[3]Department of Pathology, Nagoya University Graduate School of Medicine, Nagoya, Aichi, 466-8550, Japan

[4]Division of Molecular Pathology, Center for Neurological Disease and Cancer, Nagoya University Graduate School of Medicine, Nagoya, Aichi, 466-8550, Japan

[5]Department of Molecular Pathology, Graduate School of Medicine, Fujita Health University, Toyoake, Aichi, 470-1192, Japan

[6]Department of Gastroenterology and Hepatology, Nagoya University Graduate School of Medicine, Nagoya, Aichi, 466-8550, Japan

Correspondence: D.L.W.; dan@colonoscopyclinic.com.au, Group Leader, Gut Health, SAHMRI Address: SAHMRI (5 South), North Terrace, Adelaide SA 5000, AUSTRALIA, 08-8128-4386, S.L.W.; susan.woods@adelaide.edu.au, Group Leader, Gut Cancer, the University of Adelaide, Address: SAHMRI (5 South), North Terrace, Adelaide SA 5000, AUSTRALIA, 08-8128-4386, A.E.; enomoto@iar.nagoya-u.ac.jp, Professor, Department of Pathology, Nagoya University School of Medicine, Address: 65 Tsurumai-Cho, Showa-Ku, Nagoya, 466-8550, JAPAN, 05-2744-2093.

Author Contributions

H.K., K.A.G., T.R.L., S.A., A.E., M.T., T.C.W., S.L.W., and D.L.W. conceived and designed the study. H.K., K.A.G., and T.R.L. performed most of the experiments. H.K. and T.W. (Tongtong Wang) performed statistical analyses. T.W. and H.K. analyzed RNA-seq and microarray datasets. Y.M., T.I, R.A., and A.S. performed smFISH. N.A. and A.E.S. performed animal experiments using *Isl*r-CreERT2 and *Krt19*-Cre mice, respectively. E.M.T., J.G., and G.R. performed *Lepr*-lineage tracing experiments in a colonic injection model. S.K. and M.L.B. collected and provided human CRC clinical data and samples. H.K., K.A.G., and T.R.L. performed histopathological analyses. H.K. and K.A.G. performed experiments with *Mcam*-KO mice. N.A., S.A., A.D.B., M.T., A.E., S.L.W., and D.L.W. supervised the project. H.K., A.E., S.L.W., and D.L.W. wrote the manuscript. All authors contributed substantially to the discussion of content for the article, reviewed and/or edited the manuscript before submission.

*These authors contributed equally.

Disclosures

F.R. is a consultant to or on the advisory board of Agomab, Allergan, AbbVie, Boehringer-Ingelheim, Celgene/BMS, CDISC, Cowen, Genentech, Gilead, Gossamer, Guidepoint, Helmsley, Index Pharma, Jannsen, Koutif, Mestag, Metacrine, Morphic, Origo, Pfizer, Pliant, Prometheus Biosciences, Receptos, RedX, Roche, Samsung, Surrozen, Takeda, Techlab, Theravance, Thetis, and UCB. The remaining authors disclose no conflicts.

Transcript Profiling: GSE162508

[7]Department of Gastroenterology, Graduate School of Medicine, The University of Tokyo, Tokyo, 113-0033, Japan

[8]Colorectal Unit, Department of Surgery, Royal Adelaide Hospital, Adelaide, SA, 5000, Australia.

[9]Department of Anatomical Pathology, Flinders Medical Centre, Bedford Park, Adelaide, SA, 5001, Australia

[10]Pathology and Laboratory Medicine, Schulich School of Medicine & Dentistry, University of Western Ontario, London, ON, Canada

[11]Department of Medicine, University of Western Ontario, London, ON, Canada

[12]Envoi Specialist Pathologists, Kelvin Grove 4059, Queensland, Australia

[13]Faculty of Medicine, University of Queensland, Herston 4006, Queensland, Australia

[14]QIMR Berghofer Medical Research Institute, Herston 4006, Queensland, Australia

[15]Department of Gastroenterology, Hepatology, and Nutrition, Digestive Diseases and Surgery Institute, Cleveland Clinic Foundation, Cleveland, Ohio, USA

[16]Department of Inflammation and Immunity, Lerner Research Institute, Cleveland Clinic Foundation, Cleveland, Ohio, USA

[17]Department of Microbiology and Immunology, Vagelos College of Physicians and Surgeons, Columbia University, New York, NY, USA.

[18]Herbert Irving Comprehensive Cancer Center, Columbia University, New York, NY, USA.

[19]Department of Biomedical Engineering, Columbia University, New York, NY, USA

[20]Translational and Clinical Research Institute, Newcastle University, Newcastle upon Tyne NE2 4HH, UK

[21]Intestinal Stem Cell Biology Lab, Wellcome Trust Centre Human Genetics, University of Oxford, Oxford, UK

[22]Department of Medicine and Irving Cancer Research Center, Columbia University, New York, NY, USA

[23]International Center for Cell and Gene Therapy, Fujita Health University, Toyoake, Aichi, 470-1192, Japan

[24]GastroIntestinal Endoscopy, Lutwyche 4030, Queensland, Australia

[25]Co-corresponding authors

[26]Lead contact

Abstract

Background and aims—Cancer-associated fibroblasts (CAFs) play an important role in colorectal cancer (CRC) progression and predict poor prognosis in CRC patients. However, the cellular origins of CAFs remain unknown, making it challenging to therapeutically target these

cells. Here, we aimed to identify the origins and contribution of colorectal CAFs associated with poor prognosis.

Methods—To elucidate CAF origins, we used a colitis-associated CRC mouse model in 5 different fate-mapping mouse lines with BrdU dosing. RNA-sequencing of fluorescence-activated cell sorting (FACS)-purified CRC CAFs was performed to identify a potential therapeutic target in CAFs. To examine the prognostic significance of the stromal target, CRC patient RNA-sequencing data and tissue microarray were used. CRC organoids were injected into the colon of knockout mice to assess the mechanism by which the stromal gene contributes to colorectal tumorigenesis.

Results—Our lineage-tracing studies revealed that, in CRC, many ACTA2$^+$ CAFs emerge through proliferation from intestinal pericryptal Leptin receptor (*Lepr*)$^+$ cells. These *Lepr*-lineage CAFs, in turn, express melanoma cell adhesion molecule (MCAM), a CRC stroma-specific marker we identified using RNA-sequencing. High MCAM expression induced by TGF-β was inversely associated with patient survival in human CRC. In mice, stromal *Mcam* knockout attenuated orthotopically injected colorectal tumoroid growth and improved survival through decreased tumor-associated macrophage recruitment. Mechanistically, fibroblast MCAM interacted with interleukin-1 receptor 1 to augment nuclear factor-κB-IL34/CCL8 signaling that promotes macrophage chemotaxis.

Conclusion—In colorectal carcinogenesis, pericryptal *Lepr*-lineage cells proliferate to generate MCAM$^+$ CAFs that shape the tumor-promoting immune microenvironment. Preventing the expansion/differentiation of *Lepr*-lineage CAFs or inhibiting MCAM activity could be effective therapeutic approaches for CRC.

Graphical Abstract

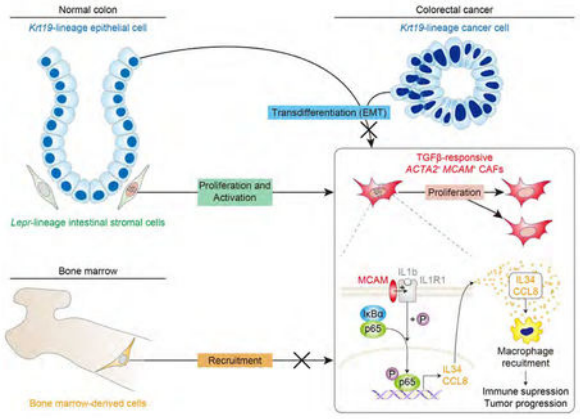

Lay Summary

In colorectal cancer (CRC), tissue-resident *LepR*-lineage stromal cells are a major contributor to MCAM$^+$ immunoregulatory cancer-associated fibroblasts. Understanding this stromal evolution has uncovered novel potential therapeutic targets for CRC.

Keywords

colorectal cancer; tumor microenvironment; alpha-smooth muscle actin (αSMA); CD146

Introduction

Colorectal cancer (CRC) is a leading cause of cancer-related death. Cancer-associated fibroblasts (CAFs) are histologically prominent and biologically important in CRC initiation, progression, and metastasis[1]. CAFs contribute to carcinogenesis via secretion of growth factors, cytokines, pro-angiogenic factors, and extracellular matrix[1]. Recent studies using immunophenotyping and single-cell RNA-sequencing (scRNA-seq) have revealed that CAFs contain heterogeneous subpopulations[2]. It is now apparent that distinct CAF populations have different consequences on cancer growth. Some CAFs promote while others retard cancer growth[3]. The cellular origins of CAFs, whether promoting or retarding, are poorly understood[1]. With respect to the development and consequences of CAFs on CRC growth, there remain at least three unresolved questions. Firstly, are CAFs newly generated cells arising through proliferation, or simply old cells acquiring a new phenotype? Secondly, if any of the CAFs emerge through proliferation, what is their cellular origin? Thirdly, what CAF-derived factors promote cancer progression, and could those be targeted with novel stromal therapies?

Theoretically, CAFs could arise through at least four non-mutually exclusive mechanisms; ***proliferation (A)***, ***activation (B)***, ***transdifferentiation (C)***, and ***recruitment (D)***[1]. Although studies using autochthonous mouse models of cancers have indicated that some CAFs undergo proliferation ***(A; Proliferation)***[4, 5], the relative contribution of proliferating and non-proliferating CAFs to the entire pool remains unclear. Induced by factors such as transforming growth factor β (TGF-β)[6], quiescent fibroblasts might undergo phenotypic conversion into activated CAFs, an old cell, but with a new mask ***(B; Activation)***. Thirdly, several fate-mapping studies have indicated that non-fibroblast lineage cells, such as epithelial cells, could transdifferentiate into CAFs through epithelial-to-mesenchymal transition (EMT) ***(C; Transdifferentiation)***[7]. Lastly, bone marrow transplantation experiments have indicated that about 20% of ACTA2 (Protein name, alpha-smooth muscle actin; αSMA)$^+$ CAFs were recruited from the bone marrow in a mouse model of gastric cancer ***(D; Recruitment)***[8]. Human studies have also suggested that bone marrow contribution can be detected in CAFs in several neoplasias including colorectal[9]. Others, however, have suggested that local precursors were a predominant contributor to ACTA2$^+$ CAFs[10]. Thus, the origin of CAFs remains uncertain. In contrast to fibrosis in organs such as the liver, kidney, and skin, in which the origins of myofibroblasts have been extensively investigated[11], to our knowledge, no previous CAF studies have comprehensively performed lineage-tracing experiments to track the aforementioned four possible CAF sources.

Leptin receptor (*Lepr)* is a well-established marker for perivascular mesenchymal cells, which support bone marrow hematopoietic stem cell (HSC) maintenance[12]. Previous fate-mapping studies have demonstrated that *Lepr*-expressing cells give rise to bone and adipocytes formed in the adult normal bone marrow[13] as well as myofibroblasts in primary myelofibrosis[14]. However, the significance of *Lepr*-lineage cells in the development of CAFs is unknown.

Similar to *Lepr*, MCAM (melanoma cell adhesion molecule, also known as CD146 or MUC18) is highly expressed by perivascular stromal cells in the bone marrow and suggested to be important in the HSC niche[15]. MCAM is also expressed by endothelial cells, melanoma cells, pericytes, and CAFs[16, 17]. MCAM expressed in endothelial and melanoma cells contributes to cancer progression by promoting cancer cell growth, angiogenesis, and metastasis[17, 18]. Recently, scRNA-seq analyses have revealed that *MCAM* defines a subset of pericyte-like CAFs that secrete tumor-promoting immunomodulatory cytokines in human cholangiocarcinoma and breast cancer[19, 20]. The biological role of $MCAM^+$ CAFs, however, has been poorly defined in CRC.

This study, for the first time, comprehensively addresses the cellular origins, dynamics, and consequences of specific CAFs in CRC. Using lineage tracing, we identify intestinal pericryptal *Lepr*-lineage cells as a major source of proliferating CAFs in a mouse model of CRC. Next, by combining fluorescence-activated cell sorting (FACS), RNA-sequencing (RNA-seq), and immunohistochemistry, we show these CAFs express MCAM. We investigate the clinical significance of MCAM expression using RNA-seq data and tissue microarray from human CRC samples. Finally, we uncover the mechanism of stromal MCAM action in CRC using newly generated *Mcam*-null mice and mouse colonoscopy.

Materials and Methods

Statistical analysis

Comparison of 2 groups was performed using two-tailed unpaired t-tests or Mann–Whitney U tests. For multiple comparisons, we used analysis of variance (ANOVA) or Kruskal-Wallis test. For survival analyses, Kaplan-Meier survival estimation with a Log-rank (Mantel-cox) test was performed. Statistical analyses were conducted using GraphPad Prism 8.00 (GraphPad) or SPSS Statistics ver. 25 (IBM). P-values of less than 0.05 were considered statistically significant.

For all other Materials and Methods, see Supplementary Materials.

Results

Desmoplasia is increased during colorectal carcinogenesis in human and mice.

To explore whether desmoplasia is increased during colorectal carcinogenesis and identify a suitable mouse model to investigate this, we performed immunohistochemistry for ACTA2, a well-established marker for CAFs, in human colorectal samples. The ratio of $ACTA2^+$ fibroblasts in the total stromal cells increased from normal to low-grade adenoma to high-grade adenoma, and ultimately adenocarcinoma (Figure 1A and B). The elevated ACTA2 expression level during colorectal carcinogenesis was corroborated by an analysis of expression microarray data from human colorectal tissues (Supplementary Figure 1A). Analyses of scRNA-seq data from human CRC tissues[2] also demonstrated that *ACTA2* expression is increased in CAFs compared with normal fibroblasts, with the highest *ACTA2* transcripts observed in pericytes among various CAF subpopulations (Figure 1C; Supplementary Figure 1B and C).

Next, we investigated the prognostic significance of *ACTA2* expression in The Cancer Genome Atlas (TCGA) data. High *ACTA2* expression was inversely associated with overall survival in patients with CRC (Figure 1D). High *ACTA2* expression, as well as high expression of *FAP*, an activated fibroblast marker[1], was consistently associated with poor prognosis across multiple expression datasets from CRC patients (Supplementary Figure 2). The highest *ACTA2* expression was observed in the poor-prognosis stroma-rich molecular subtype of CRC (Consensus Molecular Subtype 4; CMS4)[21] (Figure 1E).

We then sought to explore whether ACTA2$^+$ fibroblasts are similarly increased in mouse models of CRC. To this end, we performed ACTA2 immunohistochemistry using tumors from the azoxymethane (AOM)/dextran sulfate sodium (DSS) (Figure 1F and G) and *Apc*$^{Min/+}$ mouse models. In line with a previous study[22], ACTA2 expression was significantly elevated in the stroma of AOM/DSS tumors compared with the adjacent normal mucosa (Figure 1H and I). Similarly, small intestinal tumors from *Apc*$^{Min/+}$ mice showed an increase in stromal ACTA2 expression in comparison with the adjacent normal tissue, but to a lesser extent than the AOM/DSS mouse model (Supplementary Figure 3A and B). Taken together, these data suggest that *ACTA2*$^+$ fibroblast number increases throughout colorectal carcinogenesis in humans, and this is recapitulated in the AOM/DSS mouse model of CRC.

A subpopulation of CRC CAFs arises through proliferation in human and mice.

We next addressed the question of whether CAFs emerge through cell division or simply increase ACTA2 expression in existing cells. Co-staining for ACTA2 and Ki67 using human colorectal samples revealed that the percentage of ACTA2 and Ki67 double-positive cells (i.e., proliferating ACTA2$^+$ CAFs) was increased in high-grade adenoma and adenocarcinoma compared to normal colorectal mucosa, with about 10% of ACTA2$^+$ CAFs marked by Ki67 in adenocarcinoma (Figure 2A and B). Analysis of scRNA-seq data from human CRC and normal mucosa[2] confirmed that a subcluster of *ACTA2*$^+$ CAFs expressed *MKI67*, and this co-expressing population was not found in fibroblasts from the normal mucosa (Supplementary Figure 4A–C). These data suggest that human CRC CAFs undergo mitosis during malignant progression.

Ki67 only temporarily marks actively cycling cells, so our analysis of proliferation of human CRC CAFs may underestimate CAFs that divided at an earlier time-point. To capture the entire population of CAFs that underwent proliferation during carcinogenesis, we took advantage of continuous 5-bromodeoxyuridine (BrdU) labeling in the AOM/DSS mouse model. After the last course of DSS/water treatment (5-day DSS treatment followed by a 16-day recovery period with normal drinking water), BrdU dosing commenced at the onset of observable tumors (Figure 2C). The ratio of ACTA2$^+$ fibroblasts that incorporated BrdU was significantly elevated in AOM/DSS tumors, compared to the adjacent non-neoplastic colon, with approximately 75% of ACTA2$^+$ fibroblasts in AOM/DSS tumors marked by BrdU (Figure 2D and E; Supplementary Figure 5). Colonoscopic and microscopic evaluation of AOM/DSS tumors confirmed the absence of excavated ulcers or severe inflammation at the time point when BrdU labeling started (Figure 2C; Supplementary Figure 6). These data indicate that ACTA2$^+$ fibroblasts have divided during AOM/DSS tumorigenesis, after DSS-induced acute colitis subsided. Contrasting with the BrdU incorporation ratio, the

ratio of actively proliferating fibroblasts ($Ki67^+ACTA2^+$ fibroblasts) in the total pool of $ACTA2^+$ fibroblasts was only about 1.5% in AOM/DSS tumors and was not significantly different from the ratio of proliferating fibroblasts in the normal mouse colorectal mucosa (Figure 2D and E). Collectively, our data suggest that, in AOM/DSS tumors, the majority of $ACTA2^+$ fibroblasts at humane endpoint were in quiescent G0 phase as evaluated by Ki67 negativity, but approximately three-fourths of the fibroblasts had undergone cell division and incorporated BrdU during colitis-associated tumorigenesis after the last DSS/recovery cycle.

Lepr-lineage stromal cells are a major contributor to the proliferating fibroblasts in AOM/DSS CRC.

We next sought to establish the cellular origin of the proliferating fibroblasts in AOM/DSS tumors by using a lineage-tracing strategy. We selected transgenic mouse lines that **(1)** identified putative colorectal mesenchymal stem-progenitor cells (*Lepr*-Cre; Rosa26-LSL-tdtomato[12], *Grem1*-CreERT2; Rosa26-LSL-ZsGreen[23] and *Islr*-CreERT2; Rosa26-LSL-tdtomato[3] or **(2)** labeled epithelium (*Krt19*-Cre; Rosa26-mt/mG) or **(3)** marked bone marrow-derived cells through a combination of bone marrow from *Acta2*-RFP mouse transplanted into non-RFP recipients (Figure 3A–E). These fate-mapping experiments were coupled with BrdU labeling beginning at the onset of observable tumors after the last DSS/recovery cycle (Figure 2C). Tamoxifen was administered to the inducible Cre lines at postnatal day 6.

Immunofluorescence for EPCAM, a pan-epithelial cell marker, showed that all *Lepr*-, *Grem1*-, and *Islr*-lineage cells were observed only within the $EPCAM^-$ stroma, validating their mesenchymal identity (Figure 3A). In AOM/DSS tumors, approximately half of $ACTA2^+$ fibroblasts and 75% of proliferating $BrdU^+ACTA2^+$ fibroblasts were *Lepr*-lineage-positive, with a smaller proportion of $ACTA2^+$ fibroblasts derived from the *Grem1*-lineage and *Islr*-lineage (Figure 3A and C–E). *Lepr*-lineage cells represented about 47.1% and 17.4% of the total $PDGFRA^+$ fibroblasts in the AOM/DSS tumors and normal colons, respectively (Supplementary Figure 7A and B). Together, these results suggest that *Lepr*-lineage stromal cells are a major source of proliferating $ACTA2^+$ fibroblasts during AOM/DSS carcinogenesis.

***Lepr*-lineage cells contribute to $ACTA2^+$ proliferating CAFs in a CRC organoid transplantation model.—**We next asked whether *Lepr*-lineage cells also give rise to proliferating $ACTA2^+$ CAFs in a distinct model of CRC. To this end, we colonoscopically injected $Apc^{\Delta/\Delta}$, $Kras^{G12D/\Delta}$, $Trp53^{\Delta/\Delta}$ mouse CRC organoids (hereafter termed AKP tumoroids) into the colon of *Lepr*-Cre; Rosa26-LSL-tdtomato mice (Supplementary Figures 8A–D and 9A). Continuous BrdU dosing commenced one day after tumoroid transplantation. In this model, approximately 72% of $ACTA2^+$ CAFs underwent proliferation as assessed by BrdU positivity (Supplementary Figure 9B and C). Similar to our findings with the AOM/DSS model, *Lepr*-lineage cells were a major contributor to $BrdU^+ACTA2^+$ CAFs in this model, with 53% of the proliferating CAFs derived from *Lepr* lineage (Supplementary Figure 9B, D, and E). Our *Lepr*-lineage tracing data from colitis-associated and sporadic CRC models suggest that the majority of proliferating $ACTA2^+$ CAFs in CRC originate from *Lepr*-lineage cells.

Neither epithelium nor bone marrow recruitment contributed to ACTA2$^+$ CAFs in the AOM/DSS mouse model of CRC.

We explored whether colonic epithelial cells could undergo epithelial-mesenchymal transition into colorectal CAFs. For this purpose, we utilized constitutive *Krt19*-Cre; Rosa26-mt/mG mice to track the fate of *Krt19*-lineage colonic epithelial cells. All colonic cells with epithelial morphology were marked following reporter recombination by Cre recombinase driven by the *Krt19* promoter (Figure 3B). However, no *Krt19*-lineage cells were positive for ACTA2 in either normal colon or AOM/DSS tumors (Figure 3B and D). This suggests that, at least in this mouse model of CRC, the epithelium is not a source of ACTA2$^+$ CAFs.

Next, to assess the contribution of bone marrow-derived cells to the AOM/DSS tumor stroma, we performed bone marrow transplantation experiments using an *Acta2*-RFP (red fluorescent protein) reporter mouse as a donor. Initially, we validated that, in *Acta2*-RFP mice that did not undergo bone marrow transplantation, RFP was expressed by fibroblastic cells in AOM/DSS tumors, confirming that the *Acta2* promoter is active in this CRC mouse model (Supplementary Figure 10A and B). To perform bone marrow transplantation from *Acta2*-RFP mice, wild-type recipient mice were subjected to total body irradiation and transplanted with whole bone marrow cells from *Acta2*-RFP donor mice. Then, the mice were treated with AOM/DSS to induce colorectal tumors (Supplementary Figure 11A). Quantitative polymerase chain reaction (qPCR) for RFP using genomic DNA isolated from the bone marrow of the recipient mice confirmed engraftment of RFP$^+$ cells in the recipient bone marrow (Supplementary Figure 11B). Transplanted *Acta2*-RFP$^+$ cells were also observed in the small intestine of the wild-type recipients, further validating the engraftment (Supplementary Figure 11C). However, no bone marrow-transplanted RFP$^+$ cells were observed in AOM/DSS tumors in wild-type recipient mice (Figure 3B and D). This indicates that, at least in this experimental CRC model, CAFs did not arise via recruitment from the bone marrow, but only from local precursors.

Collectively, our data with five distinct genetically engineered mouse models suggest that tissue-resident *Lepr*-lineage stromal cells are a key contributor to the ACTA2$^+$ CAFs in AOM/DSS tumors.

Lepr-lineage intestinal stromal cells undergo proliferation and differentiation into ACTA2$^+$ CAFs during AOM/DSS carcinogenesis.

We next sought to characterize *Lepr*-lineage cells in the normal colon and AOM/DSS tumors. In the normal colonic mucosa, pericryptal *Lepr*-lineage cells were preferentially located near the base of the crypts (Figure 3F and G). *Lepr*-lineage stromal cells in AOM/DSS tumors exhibited higher ACTA2 positivity than *Lepr*-lineage stromal cells in the normal mucosa, indicating that *Lepr*-lineage cells underwent phenotypic conversion into ACTA2$^+$ CAFs during carcinogenesis (Supplementary Figure 12A and B). BrdU labeling in AOM/DSS-treated mice revealed that *Lepr*-lineage cells showed higher proliferation in AOM/DSS tumors, in comparison with the adjacent normal mucosa (Supplementary Figure 12C and D). Single-molecule fluorescent RNA *in situ* hybridization (smFISH) for *Lepr* revealed that active expression of *Lepr* in *Lepr*-lineage cells was reduced in the

AOM/DSS tumor compared with the normal colon (Supplementary Figure 12E and F). Together, these findings indicate that intestinal *Lepr*-lineage stromal cells undergo expansion and differentiation to ACTA2^{+} myofibroblasts at the expense of *Lepr* expression during AOM/DSS colorectal carcinogenesis.

Identification of MCAM as a CRC stroma-specific marker that defines a subset of Lepr-lineage proliferating CAFs.

Lower *Lepr* expression in the CRC mesenchyme could potentially make it challenging to therapeutically target *Lepr*-lineage CAFs based on active *Lepr* expression in established cancers. Therefore, we next aimed to identify a stromal factor that is actively expressed in the CRC mesenchyme as a potential therapeutic stromal target to treat CRC.

As a strategy to identify the most biologically relevant stromal targets, we were inspired by the parallels between cancer and developmental biology[24, 25]. For example, factors involved in fibroblast activation(e.g., TGF-β) and inflammation (e.g., nuclear-factor-κB; NF- κB) play crucial roles in both carcinogenesis and organ development[1, 25, 26]. Therefore, we decided to triangulate the fibroblastic factors that were significantly upregulated in both tumorigenesis and development compared to adult colonic fibroblasts.

We first sorted fibroblasts using a negative selection strategy. Fibroblasts were selected based on their lack of expression of blood cell markers (CD45 and Ter119), an endothelial marker (CD31) and an epithelial marker (EPCAM), from AOM/DSS tumors, developmental colon (postnatal day 14), and the normal adult colon (Figure 4A). Fibroblast markers such as *Grem1*, *Acta2*, and *Fap* were highly expressed in the FACS-sorted mesenchymal cells (CD45^{-}, Ter119^{-}, CD31^{-}, EPCAM^{-}), validating their enrichment for fibroblasts (Supplementary Figure 13). RNA-sequencing from the FACS-purified fibroblasts revealed that 342 genes were differentially upregulated in both the AOM/DSS tumors and the early postnatal colons when compared with the normal adult colon fibroblasts (Figure 4B, **Step 1**). Next, we analyzed the prognostic significance of these 342 genes by performing survival analysis using TCGA data, resulting in the selection of 46 genes that were associated with human CRC survival (Figure 4B, **Step 2**; Supplementary Table 1). Next, to focus on stroma-specific targets, using our RNA-seq data from normal adult colon and AOM/DSS tumors, we selected 18 stroma-specific genes that were upregulated in fibroblasts compared to epithelial cells (Figure 4B, **Step 3**; Supplementary Table 1). Then, to examine for genes expressed at the protein level in human CRC stroma, we interrogated human CRC immunohistochemistry data in the Human Protein Atlas database and selected 6 proteins that were highly expressed in the CRC stroma (Figure 4B, **Step 4**; Supplementary Figure 14). Finally, our immunohistochemistry data for candidate genes showed that MCAM was the only candidate that was consistently upregulated in the stroma of AOM/DSS tumors and the developmental colon, compared to the normal adult colon (Figure 4C and D; Supplementary Figure 15).

Next, we explored the stromal MCAM expression in human and mouse colorectal tissues. Analyses of scRNA-seq from human CRC tissues[2] and ulcerative colitis samples revealed that the high *MCAM* expression was observed in pericytes compared with other cell subpopulations such as endothelial cells, epithelial cells, and immune cells (Supplementary

Figure 16A and B). In AOM/DSS tumors, co-immunofluorescence for CD31, ACTA2, CD45, and EPCAM showed that approximately 45% of MCAM$^+$ cells expressed a pericyte/CAF marker, ACTA2 (Supplementary Figure 16C and D).

To characterize the cellular sources of MCAM$^+$ CAFs in CRC, we performed immunofluorescence for MCAM in the three mesenchymal fate-mapping mouse models (*Lepr*-Cre, *Grem1*-CreERT2, and *Isl1*-CreERT2 mice). Our data revealed that about 80% of MCAM$^+$ACTA2$^+$ CAFs were derived from the *Lepr*-lineage in AOM/DSS tumors (Figure 4E; Supplementary Figure 17A–D). We also co-stained MCAM and BrdU in AOM/DSS-treated mice that were administered BrdU during carcinogenesis. In keeping with previous scRNA-seq data showing that *Mcam* was highly expressed by a proliferative subpopulation of CAFs[5], more than half of the MCAM$^+$ cells were positive for BrdU, indicating that the majority of MCAM$^+$ cells arose through proliferation (Figure 4F and G). Collectively, these data indicate that MCAM identifies *Lepr*-lineage proliferating CAFs in AOM/DSS tumors.

Increased MCAM expression is associated with Consensus Molecular Subtype (CMS) 4 and predicts poor survival in patients with CRC.

We investigated the clinical significance of MCAM expression in CRC patients. Consistent with the observed upregulation of MCAM during mouse colorectal tumorigenesis, MCAM expression was increased in the human adenoma-carcinoma sequence (Figure 5A and B). Analyses of expression microarray data from human colorectal tissues also showed that *MCAM* transcripts were elevated during colorectal carcinogenesis (Supplementary Figure 18A and B). Furthermore, scRNA-seq data from human colorectal tissues[2] demonstrated that, among fibroblast subpopulations, *MCAM* expression was increased in pericytes during carcinogenesis (Supplementary Figure 18C and D).

Analyses of the TCGA dataset showed that the highest expression of *MCAM* was observed in poor-prognosis immunosuppressive CMS4 tumors (Figure 5C). Given that TGF-β signaling activation is a defining characteristic of CMS4 CRC[21], we reasoned that TGF-β might upregulate *MCAM* expression. In keeping with our hypothesis, stimulation of a mouse colonic fibroblast cell line, YH2 cells, with recombinant TGF-β1 enhanced *Mcam* transcript levels and a TGF-β target gene, *Acta2* (Figure 5D). This was rescued by co-treatment with Galunisertib, a specific inhibitor for TGF-β receptor 1. Consistent herewith, scRNA-seq analysis of human colorectal CAFs[2], as well as bulk CRC tissue analysis of TCGA and expression microarray data, showed positive correlations between *MCAM* and *ACTA2* expression (Figure 5E; Supplementary Figure 19A and B).

Next, to confirm the clinical association between MCAM expression and survival, we performed MCAM immunohistochemistry using tissue microarrays from our own independent cohort of 101 CRC patients. Consistent with a previous paper[27], high MCAM expression was an independent prognostic factor for poor overall survival in CRC patients (Figure 5F and G; Supplementary Tables 2 and 3). Moreover, analyses of four independent CRC datasets confirmed that high *MCAM* expression was inversely associated with survival (Supplementary Figure 20). Taken together, these data indicate that high MCAM expression driven, at least in part, by TGF-β, predicts poor prognosis in human CRC.

Genetic deletion of stromal *Mcam* inhibits colorectal tumorigenicity and improves survival via decreased Nuclear Factor-κB-IL34/CCL8-mediated macrophage recruitment.—Finally, to delineate the mechanism by which MCAM contributes to CRC progression, we generated *Mcam*-knockout mice using CRISPR/Cas9-mediated genome engineering (Supplementary Figures 21A) and colonoscopically injected luciferase-expressing AKP tumoroids into the colon of *Mcam*-knockout and wild-type mice (Figure 6A). In this mouse model, more than half of MCAM$^+$ cells were ACTA2$^+$ CAFs (Supplementary Figure 21B and C). Consistent with our earlier *MCAM* expression and survival analyses from human CRC, *Mcam*-knockout mice showed prolonged survival after tumoroid injection (Figure 6B). *Mcam*-knockout mice also demonstrated reduced tumoroid-derived luciferase signals by in *vivo* imaging system (IVIS), decreased tumor volumes and colonoscopic tumor scores (Figure 6C–F; Supplementary Figure 22A and B). In keeping with this, tumors from *Mcam*-KO mice showed reduced histological tumor area and Ki67 labeling (Supplementary Figure 22C–F).

Immunohistochemistry for various immune cell markers revealed that infiltration of CD68$^+$ macrophages and CD11b$^+$ myeloid-derived cells was decreased in tumors from *Mcam*-knockout mice (Figure 6G and H). This was accompanied by decreased FOXP3$^+$ regulatory T cells and increased CD8$^+$ cytotoxic T cells in *Mcam*-knockout mice (Supplementary Figure 23A and B). In our mouse model, we did not observe alterations in CD31$^+$ vasculature density or ACTA2$^+$ CAF area by *Mcam* knockout (Supplementary Figure 23C–F). Normal adult colons from *Mcam*-KO mice did not show altered Ki67 labeling, crypt density or length (Supplementary Figure 24A–D). This suggests that, in *Mcam*-KO mice, there are no pre-existing changes in normal colon morphogenesis that lead to the altered tumor size.

Consistent with our mouse immunophenotyping data, gene set enrichment analysis (GSEA) using TCGA data revealed positive enrichment of macrophage/monocyte chemotaxis genes in *MCAM*^{high} cancers compared with *MCAM*^{low} tumors (Supplementary Figure 25). We hypothesized that MCAM$^+$ CAFs might promote tumor-associated macrophage (TAM) recruitment, contributing to the immunosuppressive tumor microenvironment. To identify macrophage/monocyte chemoattractants secreted by MCAM$^+$ CAFs, we first performed differential gene expression analysis using scRNA-seq data from human CRC[2] and found that 462 genes were upregulated in *MCAM*^{high} CAFs compared to *MCAM*^{low} CAFs (Figure 6I). Next, using gene ontologies, we examined transcripts encoding cytokines and chemokines involved in macrophage/monocyte chemotaxis. This analysis identified *IL34* and *CCL8* as genes with roles in TAM recruitment that are upregulated in *MCAM*^{high} CAFs.

Next, to assess whether MCAM could promote IL34 and CCL8 expression, we overexpressed MCAM in YH2 cells by lentiviral transduction and stimulated MCAM-YH2 cells with recombinant interleukin (IL)-1β, which is known to induce IL34 and CCL8 expression in fibroblasts[28, 29]. As expected, IL-1β-treated MCAM-YH2 cells showed decreased IκBα expression, increased phosphorylation of NF-κB (p65), and enhanced luciferase signals from NF-κB-responsive elements, leading to upregulation of *Il34* and *Ccl8* (Figure 6J–L; Supplementary Figure 26). These alterations were rescued by co-treatment with IKK16, a selective inhibitor for IκB kinase. We reasoned that MCAM might act as a

co-receptor for IL-1β receptor, IL1R1, to potentiate IL-1β-NF-κB-IL34/CCL8 signaling. To this end, we lentivirally transduced YH2 cells with MCAM-hemagglutinin (HA) epitope tag or, as a control, mScarlet-HA, and performed immunoprecipitation with an anti-HA antibody. The co-immunoprecipitation revealed that MCAM interacted with IL1R1 (Figure 6M). Reciprocal co-immunoprecipitation of MYC-tagged IL1R1 using an anti-MYC antibody verified the interaction of IL1R1 with MCAM (Supplementary Figure 27). In line with our *in vitro* data, tumors from *Mcam*-knockout mice showed lower stromal expression of *Il34* and *Ccl8* (Figure 6N and O), accompanied by decreased NF-κB phosphorylation (Supplementary Figure 28A and B). In human CRC, TCGA and expression microarray data confirmed that *MCAM* expression was positively correlated with *IL34* and *CCL8*, as well as *CD68* and *ITGAM* (CD11b) expression (Supplementary Figure 29). Collectively, our data indicate that MCAM alters the immune microenvironment and accelerates CRC progression, in part, through increased TAM recruitment mediated by IL1R1-NF-κB-IL34/CCL8 signaling.

Discussion

In this study, we have shown that about 75% of ACTA2$^+$ CAFs in CRC were generated through proliferation, with the remaining 25% acquired through new or preserved ACTA2 expression in existing fibroblasts (i.e., activation). Most proliferating ACTA2$^+$ CAFs were derived from intestinal *Lepr*-lineage stromal cells. These *Lepr*$^+$ pericryptal fibroblasts are also the chief origin of proliferating MCAM$^+$ CAFs. High stromal MCAM expression is associated with poor clinical outcomes in patients with CRC. Furthermore, transgenic knockout of *Mcam* in the colorectal tumor microenvironment limits tumor growth and improves survival by modifying TAM recruitment and immune landscapes. These data suggest that MCAM, a prominent cell surface protein, could prove to be a valuable novel stromal target in the prevention and treatment of CRC.

Several previous studies have indicated that recruitment from the bone marrow could contribute to CAFs in mouse models of cancers such as gastric and breast cancer[8, 30]. In contrast, one paper demonstrated that no *Acta2*-RFP$^+$ CAFs were detected in small intestinal tumors developed in a parabiosis study of an *Apc*$^{Min/+}$ with an *Acta2*-RFP mouse[10]. In agreement with this, we found that no ACTA2$^+$ CAFs were derived from the bone marrow in an AOM/DSS model of CRC. To our knowledge, our study is the first to examine bone marrow contribution to CAFs in tumors in the mouse colon. Human studies using secondary tumors (including colorectal neoplasias) developed after sex-mismatched bone marrow transplantation also indicated that bone marrow-derived cells are not a major contributor to ACTA2$^+$ CAFs[9, 31]. It is plausible, and indeed likely, that the origins and contributions of CAFs are context-dependent, depending on cancer stage, cancer genetics, and organ-specific microenvironment.

Intestinal normal and neoplastic epithelium develop from stem-progenitor cell hierarchies[32]. Analogous to this, we have previously shown that *Grem1*$^+$ intestinal reticular stromal cells identify connective tissue stem cells in the normal small intestine[23]. Here, our data indicate that the majority of CRC CAFs, however, arise not from *Grem1*$^+$ cells, but from intestinal *Lepr*-lineage pericryptal cells. Interestingly, a recent paper found that *Gli1*$^+$ pancreatic

stellate cells could contribute to approximately half of ACTA2$^+$ CAFs in a mouse model of pancreatic cancer[33]. Further research is required to determine the hierarchical or overlapping relationship between *Lepr*-lineage and *Gli1*-lineage CAFs in different tissues in health and neoplasia.

One limitation of the present study is that we have not been able to ascertain whether *Lepr*-lineage CAFs display cellular plasticity during cancer development as has been shown to occur in cancer stem cells[32] or whether they undergo an irreversible "lineage-restricted" differentiation. Given that CAFs are considered to exhibit tumor stage-dependent phenotypes[1, 34], it is conceivable that *Lepr*-lineage CAFs could adapt to dynamic phenotypic shifts during colorectal carcinogenesis and co-evolve with epithelial genetic events.

Another limitation of this study is that we have not determined whether MCAM expression is induced by TGF-β in *Lepr*-lineage fibroblasts during colorectal tumorigenesis, despite showing that TGF-β upregulates *Mcam* expression in colonic fibroblasts *in vitro*. TGF-β signaling plays a key role in differentiation of *Tcf21*$^+$ hepatic stellate cells to ACTA2$^+$ CAFs, thereby promoting liver tumor progression[35]. Further research is warranted to investigate whether conditional knockout of a TGF-β receptor in *Lepr*-lineage cells could suppress MCAM expression and thus attenuate cancer progression in a mouse model of CRC.

This work also demonstrated that MCAM is an attractive therapeutic target that modifies the immunosuppressive milieu through augmenting NF-κB signaling, key signaling that defines inflammatory phenotypes in CAFs[6, 36, 37]. Excitingly, MCAM-neutralizing antibodies show promising results in restraining cancer progression in preclinical models, including an AOM/DSS model[17, 18]. Future research should focus on investigating whether co-treatment of the MCAM-neutralizing antibody and an immune checkpoint inhibitor could unleash a cytotoxic immune response against immunologically "cold" cancers that are resistant to immunotherapies.

In conclusion, our data show that *Lepr*-lineage intestinal stromal cells, resident at the pericryptal base in the normal colon, proliferate in colorectal carcinogenesis to generate MCAM$^+$ CAFs. We also show that MCAM is an important factor in sculpting the detrimental immune microenvironment responsible for driving colorectal carcinogenesis and the associated poor patient outcome. In the future, approaches to reduce the expansion of *Lepr*$^+$ pericryptal cells, prevent their differentiation into MCAM$^+$ CAFs, and inhibit the activity of MCAM-mediated NF-κB signaling axis in mature CAFs, may all have considerable clinical value in the treatment of colorectal cancer.

Supplementary Material

Refer to Web version on PubMed Central for supplementary material.

Acknowledgments

We thank Kaori Ushida, Kozo Uchiyama (Nagoya University, JAPAN) for their technical assistance. The mouse colonic fibroblast cell line, YH2, was a kind gift from Professor Antony Burgess (Walter and Eliza Hall Institute of Medical Research, Australia). We acknowledge the facilities and the scientific and technical assistance of the

South Australian Genome Editing (SAGE) Facility, the University of Adelaide, and the South Australian Health and Medical Research Institute. SAGE is supported by Phenomics Australia. Phenomics Australia is supported by the Australian Government through the National Collaborative Research Infrastructure Strategy (NCRIS) program.

Grant Support

This study was supported by grants from the National Health and Medical Research Council (APP1156391 to D.L.W., S.L.W.) (APP1081852 to D.L.W., APP1140236 to SLW, APP1099283 to DLW,); Cancer Council SA Beat Cancer Project on behalf of its donors and the State Government of South Australia through the Department of Health (MCF0418 to S.L.W., D.L.W., and PRF1117 to L.M.B.); a Grant-in-Aid for Scientific Research (S) (26221304 to M.T.) commissioned by the Ministry of Education, Culture, Sports, Science and Technology of Japan; AMED-CREST (Japan Agency for Medical Research and Development, Core Research for Evolutional Science and Technology; 20gm0810007h0105 and 20gm1210009s0102 to A.E.); the Project for Cancer Research and Therapeutic Evolution (P-CREATE) from AMED (20cm0106377h0001 to A.E. and 21cm0106704h0002 to Y.M.); Japan Society for the Promotion of Science Overseas Challenge Program for Young Researchers (to H.K.), Takeda Science Foundation Fellowship (to H.K.), Greaton International Ph.D. Scholarship (to H.K.), Lions Medical Research Foundation Scholarship (to K.G.).

Abbreviations

ANOVA	analysis of variance
AOM	azoxymethane
CAFs	cancer-associated fibroblasts
CMS	consensus molecular subtype
CRC	colorectal cancer
DSS	dextran sodium sulfate
FACS	fluorescence-activated cell sorting
IF	immunofluorescence
IHC	immunohistochemistry
qRT-PCR	quantitative reverse-transcription polymerase chain reaction
scRNA-seq	single-cell RNA-sequencing
smFISH	single-molecule fluorescent *in situ* hybridization
TGFβ	transforming growth factor β

References

Author names in bold designate shared co-first authorship.

1. Kobayashi H, Enomoto A, Woods SL, et al. Cancer-associated fibroblasts in gastrointestinal cancer. Nat Rev Gastroenterol Hepatol 2019;16:282–295. [PubMed: 30778141]
2. Lee HO, Hong Y, Etlioglu HE, et al. Lineage-dependent gene expression programs influence the immune landscape of colorectal cancer. Nat Genet 2020;52:594–603. [PubMed: 32451460]
3. Kobayashi H, Gieniec KA, Wright JA, et al. The Balance of Stromal BMP Signaling Mediated by GREM1 and ISLR Drives Colorectal Carcinogenesis. Gastroenterology 2021;160:1224–1239 e30. [PubMed: 33197448]

4. Ozdemir BC, Pentcheva-Hoang T, Carstens JL, et al. Depletion of carcinoma-associated fibroblasts and fibrosis induces immunosuppression and accelerates pancreas cancer with reduced survival. Cancer Cell 2014;25:719–34. [PubMed: 24856586]
5. Bartoschek M, Oskolkov N, Bocci M, et al. Spatially and functionally distinct subclasses of breast cancer-associated fibroblasts revealed by single cell RNA sequencing. Nat Commun 2018;9:5150. [PubMed: 30514914]
6. Biffi G, Oni TE, Spielman B, et al. IL1-Induced JAK/STAT Signaling Is Antagonized by TGFbeta to Shape CAF Heterogeneity in Pancreatic Ductal Adenocarcinoma. Cancer Discov 2019;9:282–301. [PubMed: 30366930]
7. Rhim AD, Mirek ET, Aiello NM, et al. EMT and dissemination precede pancreatic tumor formation. Cell 2012;148:349–61. [PubMed: 22265420]
8. Quante M, Tu SP, Tomita H, et al. Bone marrow-derived myofibroblasts contribute to the mesenchymal stem cell niche and promote tumor growth. Cancer Cell 2011;19:257–72. [PubMed: 21316604]
9. Worthley DL, Ruszkiewicz A, Davies R, et al. Human gastrointestinal neoplasia-associated myofibroblasts can develop from bone marrow-derived cells following allogeneic stem cell transplantation. Stem Cells 2009;27:1463–8. [PubMed: 19492298]
10. Arina A, Idel C, Hyjek EM, et al. Tumor-associated fibroblasts predominantly come from local and not circulating precursors. Proc Natl Acad Sci U S A 2016;113:7551–6. [PubMed: 27317748]
11. El Agha E, Kramann R, Schneider RK, et al. Mesenchymal Stem Cells in Fibrotic Disease. Cell Stem Cell 2017;21:166–177. [PubMed: 28777943]
12. Ding L, Morrison SJ. Haematopoietic stem cells and early lymphoid progenitors occupy distinct bone marrow niches. Nature 2013;495:231–5. [PubMed: 23434755]
13. Zhou BO, Yue R, Murphy MM, et al. Leptin-receptor-expressing mesenchymal stromal cells represent the main source of bone formed by adult bone marrow. Cell Stem Cell 2014;15:154–68. [PubMed: 24953181]
14. Decker M, Martinez-Morentin L, Wang G, et al. Leptin-receptor-expressing bone marrow stromal cells are myofibroblasts in primary myelofibrosis. Nat Cell Biol 2017;19:677–688. [PubMed: 28481328]
15. Corselli M, Chin CJ, Parekh C, et al. Perivascular support of human hematopoietic stem/progenitor cells. Blood 2013;121:2891–901. [PubMed: 23412095]
16. Brechbuhl HM, Finlay-Schultz J, Yamamoto TM, et al. Fibroblast Subtypes Regulate Responsiveness of Luminal Breast Cancer to Estrogen. Clin Cancer Res 2017;23:1710–1721. [PubMed: 27702820]
17. Wang Z, Xu Q, Zhang N, et al. CD146, from a melanoma cell adhesion molecule to a signaling receptor. Signal Transduct Target Ther 2020;5:148. [PubMed: 32782280]
18. Xing S, Luo Y, Liu Z, et al. Targeting endothelial CD146 attenuates colitis and prevents colitis-associated carcinogenesis. Am J Pathol 2014;184:1604–16. [PubMed: 24767106]
19. Zhang M, Yang H, Wan L, et al. Single-cell transcriptomic architecture and intercellular crosstalk of human intrahepatic cholangiocarcinoma. J Hepatol 2020;73:1118–1130. [PubMed: 32505533]
20. Wu SZ, Roden DL, Wang C, et al. Stromal cell diversity associated with immune evasion in human triple-negative breast cancer. EMBO J 2020;39:e104063. [PubMed: 32790115]
21. Guinney J, Dienstmann R, Wang X, et al. The consensus molecular subtypes of colorectal cancer. Nat Med 2015;21:1350–6. [PubMed: 26457759]
22. Torres S, Bartolome RA, Mendes M, et al. Proteome profiling of cancer-associated fibroblasts identifies novel proinflammatory signatures and prognostic markers for colorectal cancer. Clin Cancer Res 2013;19:6006–19. [PubMed: 24025712]
23. Worthley DL, Churchill M, Compton JT, et al. Gremlin 1 identifies a skeletal stem cell with bone, cartilage, and reticular stromal potential. Cell 2015;160:269–84. [PubMed: 25594183]
24. Reichert M, Takano S, von Burstin J, et al. The Prrx1 homeodomain transcription factor plays a central role in pancreatic regeneration and carcinogenesis. Genes Dev 2013;27:288–300. [PubMed: 23355395]
25. Sancho E, Batlle E, Clevers H. Signaling pathways in intestinal development and cancer. Annu Rev Cell Dev Biol 2004;20:695–723. [PubMed: 15473857]

26. Espin-Palazon R, Traver D. The NF-kappaB family: Key players during embryonic development and HSC emergence. Exp Hematol 2016;44:519–27. [PubMed: 27132652]
27. Tian B, Zhang Y, Li N. CD146 protein as a marker to predict postoperative liver metastasis in colorectal cancer. Cancer Biother Radiopharm 2013;28:466–70. [PubMed: 23745687]
28. Struyf S, Van Collie E, Paemen L, et al. Synergistic induction of MCP-1 and −2 by IL-1beta and interferons in fibroblasts and epithelial cells. J Leukoc Biol 1998;63:364–72. [PubMed: 9500525]
29. Baghdadi M, Umeyama Y, Hama N, et al. Interleukin-34, a comprehensive review. J Leukoc Biol 2018;104:931–951. [PubMed: 30066957]
30. Raz Y, Cohen N, Shani O, et al. Bone marrow-derived fibroblasts are a functionally distinct stromal cell population in breast cancer. J Exp Med 2018;215:3075–3093. [PubMed: 30470719]
31. Kurashige M, Kohara M, Ohshima K, et al. Origin of cancer-associated fibroblasts and tumor-associated macrophages in humans after sex-mismatched bone marrow transplantation. Commun Biol 2018;1:131. [PubMed: 30272010]
32. Batlle E, Clevers H. Cancer stem cells revisited. Nat Med 2017;23:1124–1134. [PubMed: 28985214]
33. Garcia PE, Adoumie M, Kim EC, et al. Differential Contribution of Pancreatic Fibroblast Subsets to the Pancreatic Cancer Stroma. Cell Mol Gastroenterol Hepatol 2020;10:581–599. [PubMed: 32454112]
34. Friedman G, Levi-Galibov O, David E, et al. Cancer-associated fibroblast compositions change with breast cancer progression linking the ratio of S100A4+ and PDPN+ CAFs to clinical outcome. Nature Cancer 2020;1:692–708. [PubMed: 35122040]
35. Wang SS, Tang XT, Lin M, et al. Perivenous stellate cells are the main source of myofibroblasts and cancer-associated-fibroblasts formed after chronic liver injuries. Hepatology 2021.
36. Erez N, Truitt M, Olson P, et al. Cancer-Associated Fibroblasts Are Activated in Incipient Neoplasia to Orchestrate Tumor-Promoting Inflammation in an NF-kappaB-Dependent Manner. Cancer Cell 2010;17:135–47. [PubMed: 20138012]
37. Koliaraki V, Pasparakis M, Kollias G. IKKbeta in intestinal mesenchymal cells promotes initiation of colitis-associated cancer. J Exp Med 2015;212:2235–51. [PubMed: 26621453]

What you need to know

Background and context

Cancer-associated fibroblasts (CAFs) regulate colorectal cancer (CRC) progression. However, the cellular origin of CAFs and how specific CAF-lineages contribute to CRC progression is unknown.

New findings

Colonic pericryptal Leptin receptor (*LepR*)-lineage cells are a major source of $MCAM^+$ and $ACTA2^+$ CAFs. These $MCAM^+$ CAFs accelerate CRC progression via nuclear factor-κB-IL34/CCL8-mediated tumor-associated macrophage recruitment.

Limitations

This study was performed using mouse models and human tissue samples. Future studies are necessary to assess the therapeutic efficacy of targeting *LEPR*-lineage $MCAM^+$ CAFs in patients with CRC.

Impact

Inhibiting proliferation/differentiation of $LEPR^+$ cells to $MCAM^+$ CAFs or targeting mature $MCAM^+$ CAFs in established cancer are novel potential therapeutic strategies to treat CRC.

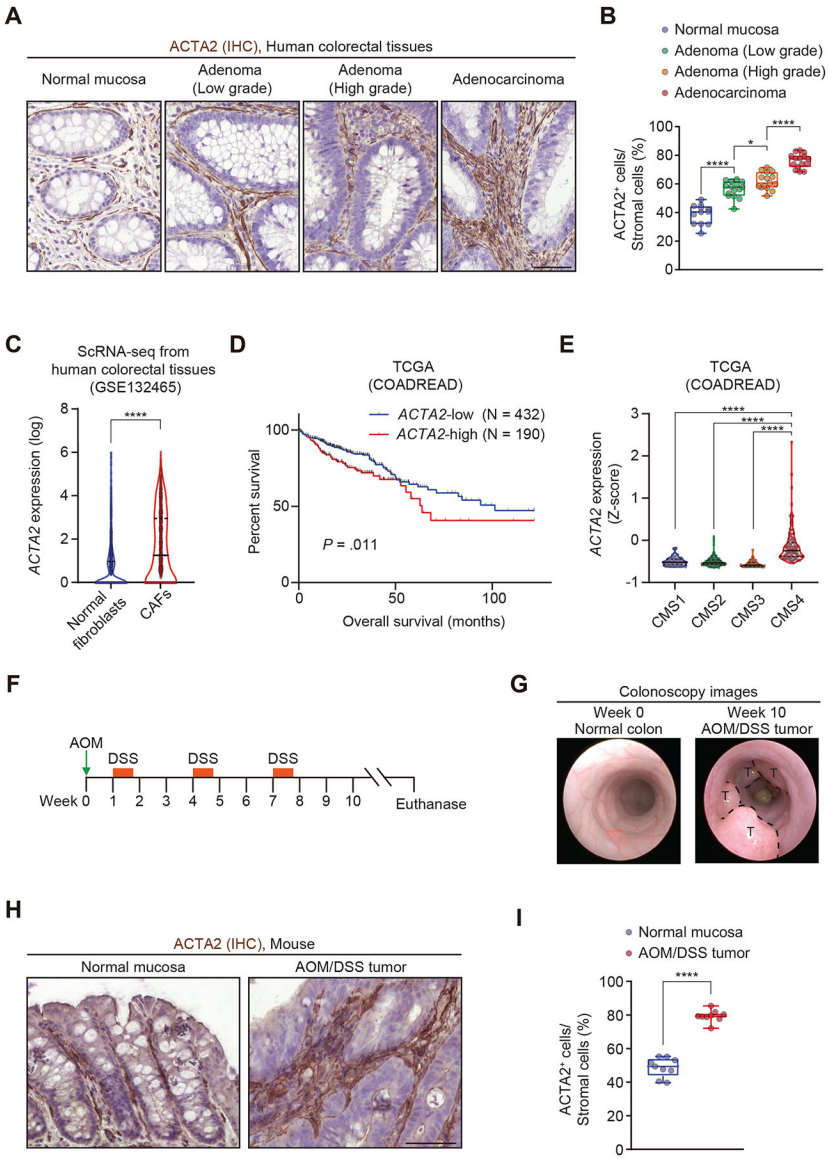

Figure 1: ACTA2 expression is increased during colorectal carcinogenesis in humans and mice.

(A, B) Immunohistochemistry (IHC) for ACTA2 in human colorectal samples. **(A)** Representative pictures. **(B)** ACTA2 positivity in total stromal cells (visualized by hematoxylin counterstaining). 3 high power fields (HPFs, 400x)/patient, 4–5 patients each.

(C) Violin plots depict *ACTA2* transcripts in normal fibroblasts (n = 2053 cells) and CRC CAFs (n = 1854 cells) assessed by single-cell RNA-sequencing (scRNA-seq) from human colorectal tissues.

(D) Kaplan-Meier survival curves in The Cancer Genome Atlas (TCGA) dataset.

(E) Violin plots showing *ACTA2* expression level in four consensus molecular subtypes (CMS). n = 76, 220, 72, and 143 patients (CMS1-4).

(F) Scheme for the experimental course of azoxymethane (AOM)/dextran sulfate sodium (DSS)-induced colorectal carcinogenesis.

(G) Representative endoscopic images of the normal colon mucosa and AOM/DSS tumors. T, tumors.

(H, I) Immunohistochemistry for ACTA2 in the normal mucosa and AOM/DSS tumors. **(H)** Representative pictures. **(I)** ACTA2 positivity in total stromal cells. 3 HPFs/mouse, 3 mice each. One-way ANOVA followed by Tukey's post-hoc multiple comparison test (B), Wilcoxon rank-sum test (C), Log-rank test (D), Kruskal-Wallis test followed by Dunn's multiple comparisons test (E), and two-tailed unpaired Student's t-test (I).

****, $P < 0.0001$; **, $P = 0.00299$; *, $P = 0.0451$.

Scale bars, 50 μm.

In all figures, box plots have whiskers of maximum and minimum values; the boxes represent first, second (median), and third quartiles. In all violin plots, solid and dotted black lines denote median and quartiles, respectively.

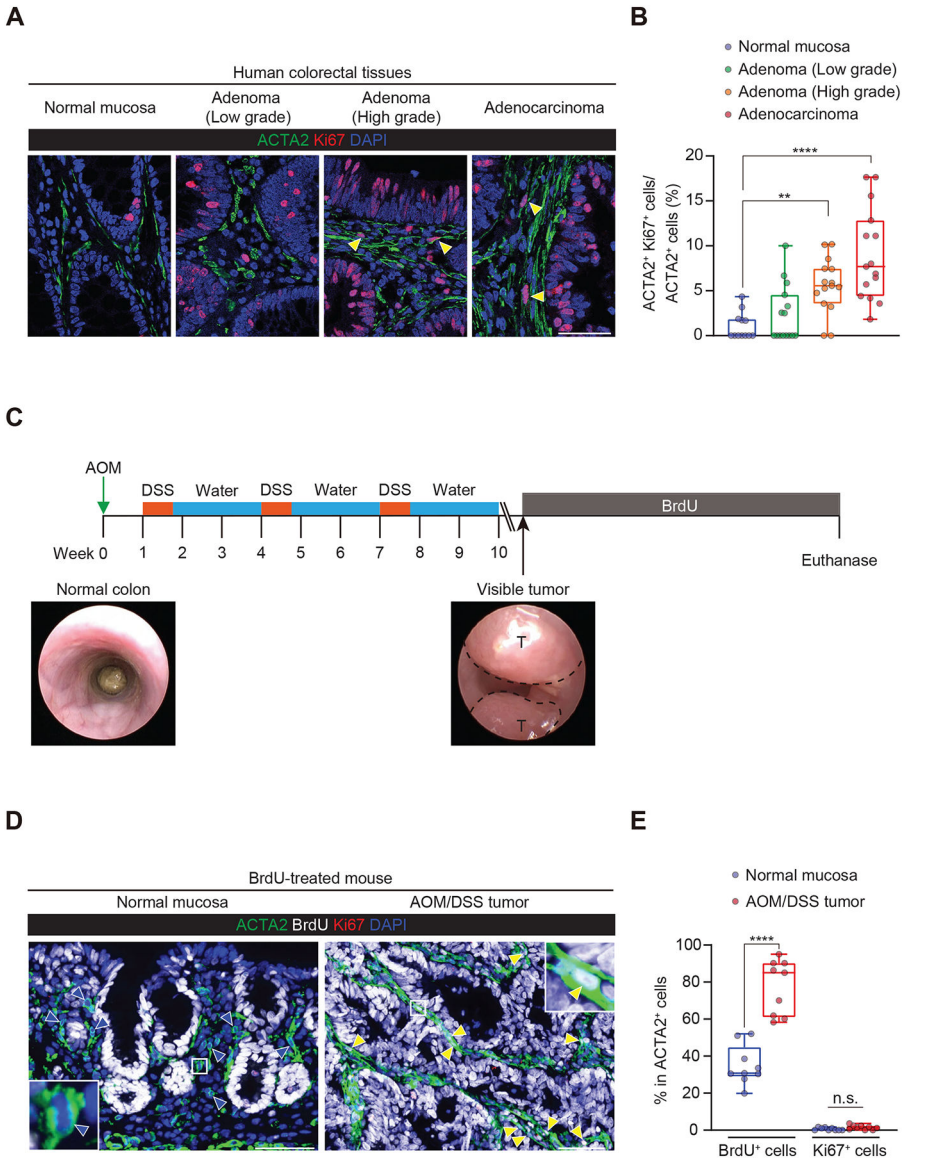

Figure 2: A subset of ACTA2$^+$ CAFs proliferate during colorectal carcinogenesis in humans and mice.

(A, B) Co-immunofluorescence for ACTA2 and Ki67 in human colorectal samples. **(A)** Representative pictures. Yellow arrowheads denote proliferating CAFs (ACTA2$^+$Ki67$^+$ cells). **(B)** Ki67 positivity in total ACTA2$^+$ cells. 3 HPFs (400x)/patient, 4–5 patients each. **(C)** Scheme for the experimental course of AOM/DSS-induced colon carcinogenesis and 5-bromodeoxyuridine (BrdU) administration. After the end of the last DSS/water cycle, continuous BrdU administration was commenced once a visible tumor was observed via mouse colonoscopy. T, tumor.

(D, E) Co-immunofluorescence for ACTA2, BrdU, and Ki67 in the normal colon mucosa and AOM/DSS tumors. **(D)** Representative images. Blue and yellow arrowheads denote ACTA2$^+$BrdU$^-$ and ACTA2$^+$BrdU$^+$ cells, respectively. **(E)** BrdU positivity (left) and Ki67 positivity (right) in total ACTA2$^+$ cells. 3 HPFs/mouse, 3 mice each.

****, P < 0.0001; **, P = 0.0077; n.s., P = 0.0857.

Kruskal-Wallis test followed by Dunn's multiple comparisons test (B) and two-tailed unpaired Student's t-test (E)
Scale bars, 50 um.

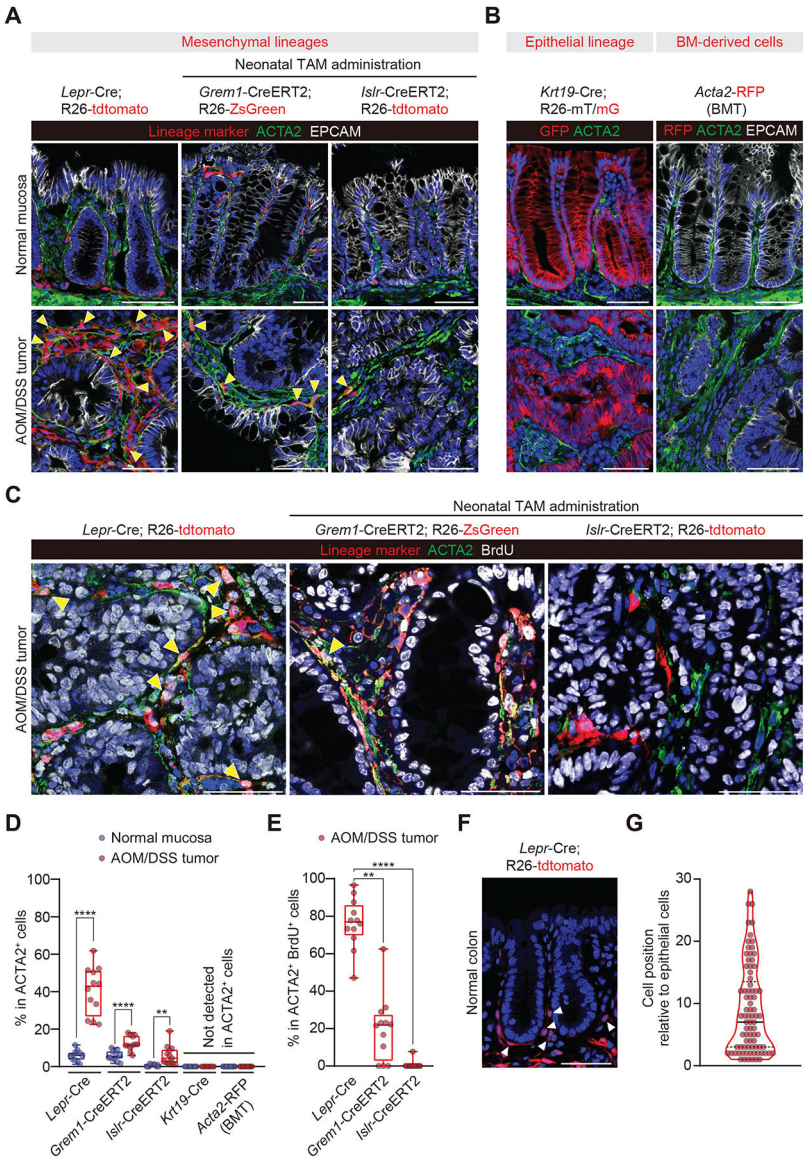

Figure 3: Proliferating ACTA2$^+$ fibroblasts in AOM/DSS tumors derive predominantly from *Lepr*-lineage cells.

(A) Immunofluorescence for ACTA2 and EPCAM in the normal colon mucosa and AOM/DSS tumors using fate-mapping mouse models. Yellow arrowheads denote lineage-marker$^+$ACTA2$^+$ cells. See Figure 3D for quantification. R26, Rosa26-loxP-stop-loxP; BM, bone marrow; BMT, bone marrow transplantation; TAM, tamoxifen.

(B) Immunofluorescence for ACTA2 in the normal mucosa and AOM/DSS tumors using *Krt19*-Cre mice. (left). Immunofluorescence for ACTA2 and EPCAM in the normal mucosa and AOM/DSS tumor, using a wild-type recipient mouse transplanted with bone marrow cells from an *Acta2*-RFP mouse (right).

(C) Immunofluorescence for ACTA2 and BrdU in AOM/DSS tumors using the BrdU-treated fate-mapping mouse models. Yellow arrowheads denote proliferating CAFs that were derived from each cellular lineage (lineage-marker$^+$ACTA2$^+$BrdU$^+$ cells).

(D) The ratio of lineage-marker$^+$ cells in total ACTA2$^+$ cells. 4 HPFs/mouse. 3 mice (*Lepr*-Cre, *Grem1*-CreERT2, *Isl1*-CreERT2, *Acta2*-RFP) and 2 mice (*Krt19*-Cre).
(E) The ratio of lineage marker$^+$ cells in total proliferating CAFs. 4 HPFs/mouse. 3 mice each.
(F, G) Cellular positions of *Lepr*-lineage stromal cells in the normal adult mouse colon. **(F)** Representative pictures. White arrowheads denote *Lepr*-lineage tdtomato$^+$ cells. **(G)** Violin plots showing the positions of pericryptal *Lepr*-lineage stromal cells relative to the adjacent epithelial position. n = 81 *Lepr*-lineage cells from 3 mice.
Scale bars, 50 μm.
Two-tailed unpaired t-test with Welch's correction (D) and Kruskal-Wallis test followed by Dunn's multiple comparisons test (E).
****, P < 0.0001; **, P = 0.0030 (D); **, P = 0.0043 (E).

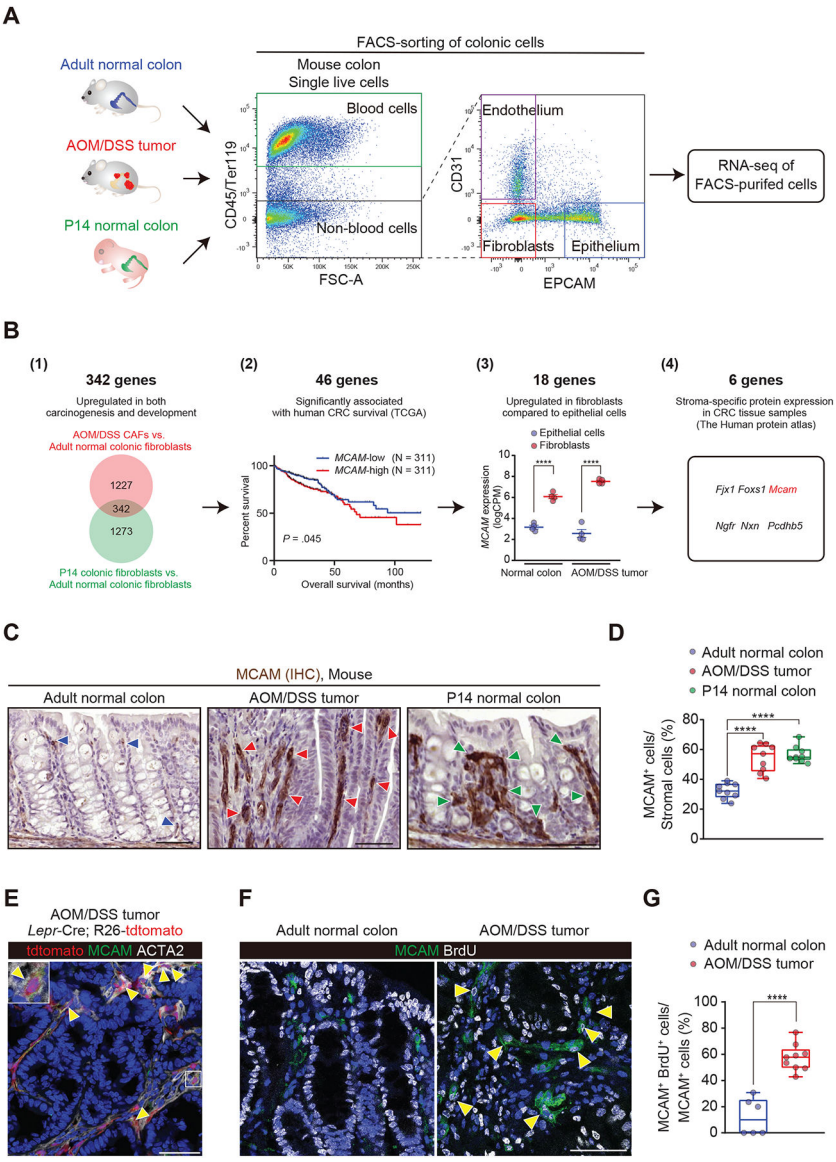

Figure 4: Identification of MCAM as a CRC mesenchyme-specific marker that represents a subset of *Lepr*-lineage proliferating cells.

(A) Experimental schematic for isolating colonic fibroblasts from the normal adult colon, AOM/DSS tumors, and postnatal day 14 colon. Gating strategy to isolate $CD45^{-}Ter119^{-}CD31^{-}EPCAM^{-}$ fibroblasts by fluorescence-activated cell-sorting (FACS) is shown for one mouse adult normal colon. n = 4 mice each.

(B) Strategy to identify a colonic stromal gene upregulated in development and carcinogenesis, which is associated with human CRC survival. **(1)** Venn diagram showing 342 genes upregulated in AOM/DSS tumors and postnatal day 14 colon, compared with the normal adult colon fibroblasts. **(2)** Survival analysis using TCGA dataset. **(3)** Using our RNA-seq data, genes upregulated in $EPCAM^{-}$ $CD31^{-}CD45^{-}Ter119^{-}$ fibroblasts compared with $EPCAM^{+}$ epithelial cells, both in the normal adult colon and AOM/DSS tumors, were selected. Mean ± s.e.m. **(4)** The Human protein atlas data were used to select genes whose protein expression was restricted to the CRC stroma. *Mcam* is highlighted in red.

(C, D) Immunohistochemistry for MCAM. **(C)** Representative images. Blue, red, and green arrowheads denote MCAM expression in the normal adult colon, AOM/DSS tumor, and postnatal day 14 colon, respectively. **(D)** The ratio of $MCAM^+$ cells in total stromal cells (visualized by hematoxylin counterstaining). 3 HPFs/mouse, 3 mice each.
(E) Co-Immunofluorescence for MCAM and ACTA2 using AOM/DSS tumors from *Lepr*-Cre; Rosa26-tdtomato mice. Yellow arrowheads denote *Lepr*-lineage $MCAM^+$ $ACTA2^+$ CAFs. See Supplementary Figure 17C and D for quantification and separate channel images.
(F, G) Co-immunofluorescence for MCAM and BrdU. **(F)** Representative images. Yellow arrowheads denote proliferating $MCAM^+$ cells. **(G)** The ratio of $MCAM^+BrdU^+$ cells in total $MCAM^+$ cells. 3 HPFs/mouse, 2–3 mice each.
Scale bars, 50 μm. ****, $P < 0.0001$. Log-rank test (B(2)), one-way ANOVA followed by Tukey's post-hoc multiple comparison test (B(3) and D), and two-tailed unpaired Student's t-test (G)

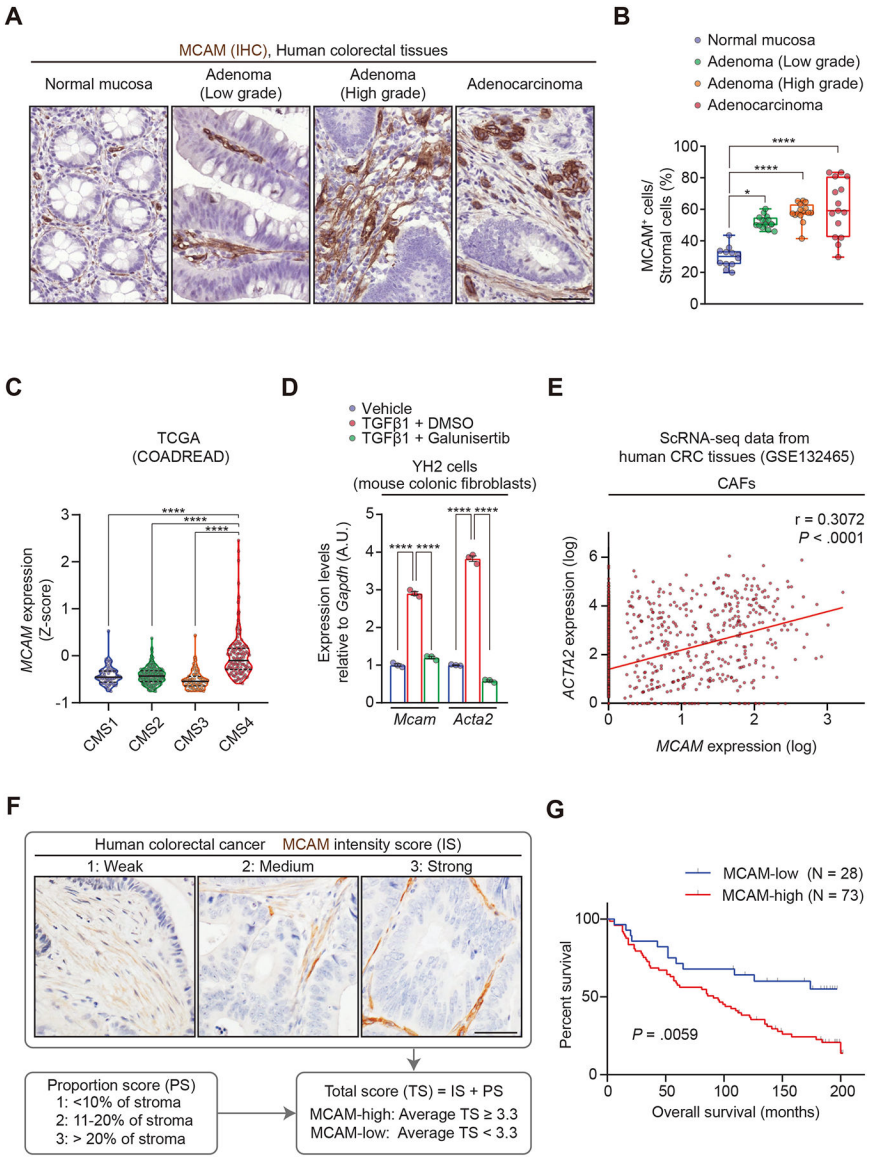

Figure 5: High stromal MCAM expression driven, in part, by TGF-β, is associated with poor survival in patients with CRC.

(A, B) Immunohistochemistry for MCAM in human colorectal samples. **(A)** Representative pictures. **(B)** MCAM positivity in total stromal cells (visualized by hematoxylin counterstaining). 3 HPFs (400x)/patient, 4–5 patients each.

(C) Violin plots showing *MCAM* expression levels in four CMSs. n = 76 (CMS1), 220 (CMS2), 72 (CMS3), and 143 patients (CMS4).

(D) A mouse colonic fibroblast cell line, YH2, was incubated with vehicle, recombinant TGFβ1, or recombinant TGFβ1 + TGFβ1-receptor inhibitor (Galunisertib) for 24 hours, followed by quantitative reverse-transcription PCR (qRT-PCR). mean ± s.e.m. n = 3.

(E) ScRNA-seq data show *MCAM* transcript levels are positively correlated with *ACTA2* expression in colorectal CAFs. n = 1854 CAFs. Solid line, linear regression

(F, G) MCAM immunohistochemistry in a CRC tissue microarray **(F)** Representative images and scoring system. **(G)** Kaplan-Meier survival curves.

Scale bars, 50 μm.

****, P < 0.0001; *, P = 0.0124.

Kruskal-Wallis test followed by Dunn's multiple comparisons test (B and C), one-way ANOVA followed by Tukey's post-hoc multiple comparison test (D), Spearman correlation (E), and Log-rank test (G).

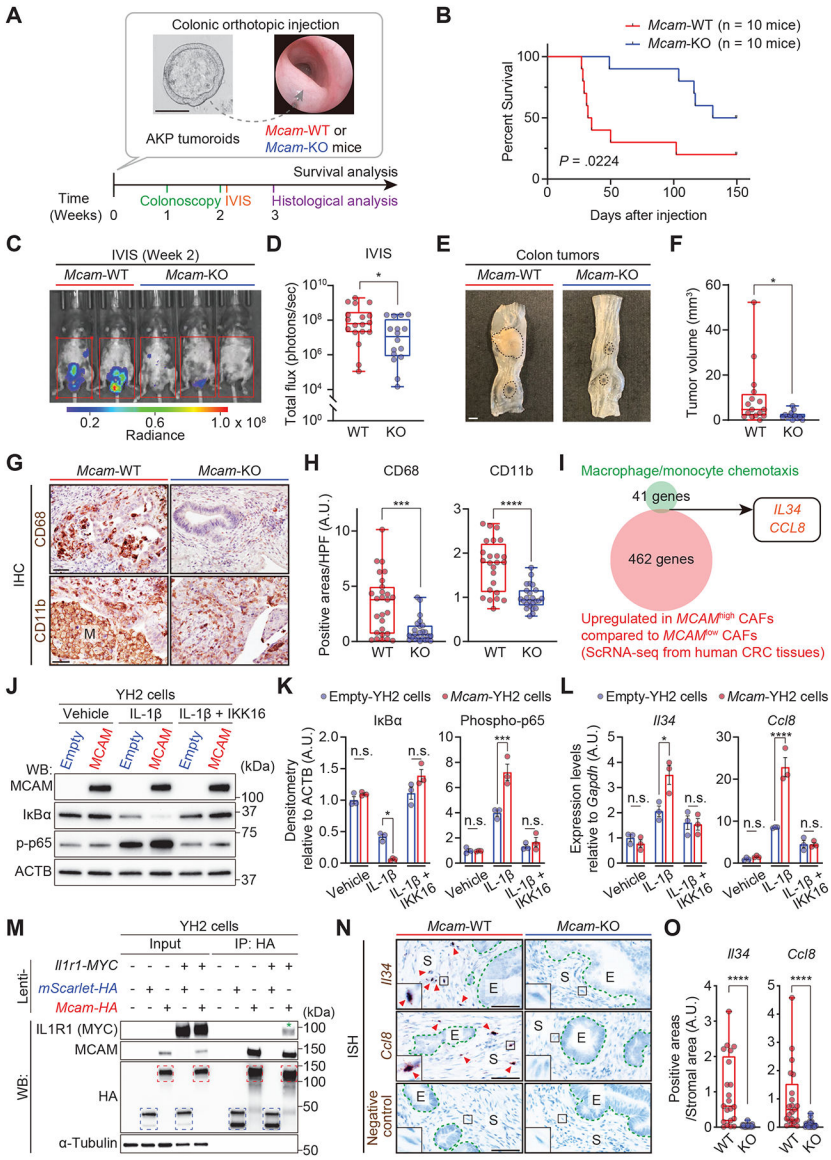

Figure 6: Stromal MCAM promotes CRC progression via IL1R1-p65-IL34/CCL8 signaling-mediated macrophage recruitment.

(A) Experimental scheme showing orthotopic injection of *Apc*$^{\Delta/\Delta}$, *Kras*$^{G12D/\Delta}$, *Trp53*$^{\Delta/\Delta}$ CRC organoids (AKP tumoroids) into the colon. WT, wild type; KO, knockout; IVIS, *in vivo* imaging system.

(B) Kaplan-Meier survival curves.

(C, D) Luciferase signals from AKP tumoroids were assessed by IVIS. 18 *Mcam*-WT and 16 KO mice.

(E, F) Macroscopic evaluation of colon tumors. Mice were harvested 3 weeks after tumoroid injection. **(E)** Representative pictures. Dotted lines indicate tumors. **(F)** Quantification of tumor volumes. 2 injections/mouse, 8 *Mcam*-WT and 6 KO mice

(G, H) Immunohistochemistry for CD68 and CD11b. **(G)** Representative pictures. M, macrophages as assessed by morphology. **(H)** 3,3'-Diaminobenzidine (DAB)-positive areas. A.U., arbitrary unit.

(I) Venn diagram showing the overlap of 41 macrophage/monocyte chemoattractant genes identified by Gene Ontologies and 462 genes upregulated in *MCAM*^{high} CAFs compared with *MCAM*^{low} CAFs (scRNA-seq data from GSE132465).

(J, K, L) Lentivirus-mediated overexpression of MCAM augments IL-1β-p65-*Il34/Ccl8* signaling in YH2 cells. MCAM-overexpressing or empty YH2 cells were stimulated with recombinant IL-1β, followed by Western blotting (WB; **J, K**) and qRT-PCR (**L**). mean ± s.e.m. n = 3 each. p-p65, phosphorylated p65.

(M) Immunoprecipitation (IP) for MCAM-hemagglutinin (HA) tag with an anti-HA antibody, followed by western blotting. A green asterisk denotes the interaction of MCAM-HA with IL1R1. An anti-MYC antibody was used to detect IL1R1 protein tagged with MYC. Blue and red dotted boxes indicate mScarlet-HA and MCAM-HA proteins, respectively.

(N, O) *In situ* hybridization (ISH) for *Il34*, *Ccl8*, and a negative control probe (bacterial *DapB* gene) **(N)** Representative pictures. Green dotted lines indicate borders between Stromal (S) and Epithelial (E) areas (visualized by hematoxylin counterstaining). Red arrowheads denote *Il34*$^{+}$ or *Ccl8*$^{+}$ stromal cells. **(O)** DAB^{+} areas in the tumor stroma. Scale bars, 200 μm (A), 2 mm (E), 50 μm (G and N)

All histopathological analyses were performed using mice harvested 3 weeks after tumoroid injection. 3 HPFs (400x)/tumor, 1–2 tumors/mouse, 5 mice each group (H and O).

Log-rank test (B), two-tailed unpaired t-test with Welch's correction (D), Mann-Whitney U-test (F, H, and O), and two-way ANOVA followed by Tukey's post-hoc multiple comparison test (K and L).

****, $P \leq 0.0001$; ***, $P \leq 0.001$; *, $P \leq 0.05$; n.s., $P > 0.05$